High frequency pulse anodising of aluminium: Anodising kinetics and optical appearance

Jensen, Flemming; Gudla, Visweswara Chakravarthy; Kongstad, Ib; Ambat, Rajan

Published in:
Surface and Coatings Technology

Link to article, DOI:
10.1016/j.surfcoat.2018.12.117

Publication date:
2019

Document Version
Peer reviewed version

High Frequency Pulse Anodising of Aluminium: Anodising Kinetics and Optical Appearance

Jensen Flemming[1,2], Gudla Visweswara Chakravarthy[1,3], Kongstad Ib [2], Ambat Rajan [1].

[1]Technical University of Denmark, Department of Mechanical Engineering, Section of Materials and Surface Engineering, Produktionstorvet, 2800 Kgs. Lyngby, Denmark

[2]Bang & Olufsen A/S, Peter Bangs Vej 15, 7600 Struer, Denmark
Email: flejen@mek.dtu.dk

[3] The University of Manchester, School of Materials, Henry Moseley X-Ray Imaging Facility, Alan Turing Building, Upper Brook Street, M13 9PY Manchester, United Kingdom

Abstract

High frequency pulsed anodising of pure aluminium was investigated with an aim to understand the effect of the anodising parameters on the growth kinetics of the anodic layer and optical appearance of the anodised surface. Anodising was performed in sulphuric acid, and the effect of the pulse duty cycle, applied potential offset, and pulse frequency was investigated. Optical properties of the anodised surfaces are improved upon lowering the anodising potential and by increasing the frequency of the applied potential pulses. Temperature evolution of the samples during anodising was investigated by employing a special flat cell setup equipped with a thermocouple close to the sample. The effect of high frequency pulsing of the anodising potential on the anodising kinetics is presented, which is related to the temperature evolution and dielectric losses, and the effect is compared to the traditional DC anodising process. From the observations, it is postulated that the dominant factor responsible for the improved growth kinetics during high frequency pulsed anodising might not be dielectric losses instead a thickness reduction in the Gouy-Chapman/Helmholtz layers.

Keywords: *Aluminium; Pulse Anodising; High Frequency; Optical Appearance; Kinetics;*

1. Introduction

Aluminium and its alloys are widely used in several industrial applications [1–5] due to their favourable strength to weight ratio, inherent corrosion resistance and passivating nature [6,7], ease of formability and recyclability [8–14], and the ability for surface modifications suiting various functional applications [15–19]. In the consumer goods industry, aluminium is often used in the anodised surface condition to impart pleasing aesthetics, higher corrosion resistance, better scratch and wear resistance, and thus an improved value of the product [20–22]. Decorative anodised surfaces are commonly produced by direct current (DC) anodising of aluminium in a sulphuric acid bath [23,24]. The resulting anodic alumina layers are hexagonally self-ordered [25,26], usually transparent to the visible light; however, the optical appearance of the anodised surface depends on the anodising parameters as well as on the Al alloy composition, and surface morphology of the substrate [27–32].

Pulse anodising of Al has been studied as an alternative technique for improving the properties and performance of the anodised surfaces on aluminium alloys with heterogeneous microstructures [33–36]. The pulse anodising technique, and its associated variations are based on the recovery effect postulated by Yokoyama et al. [37] where varying/pulsing the applied potential from a high to low value during anodising allowed for faster thickening of hard anodic coatings, while simultaneously preventing burning and powdering of the anodised surfaces. Several variations of this pulse anodising technique such as low frequency pulsing, high frequency pulsing, and pulse reverse pulsing technique were later applied by Juhl et al. [38] for anodising of both extruded and cast aluminium alloys. The hardness of the anodic layers obtained was found to be lower for the pulse reverse pulse anodised surfaces when compared to those obtained using the other two variant techniques. However, the obtained oxide structure was reported to be similar across all variants of the technique as observed using scanning electron microscopy. Ono et al. [39]

used a high frequency electrolysis technique (pulse frequency in the kHz range) for anodising cast Al-Si alloy and obtained higher uniformity of the anodic layers due to more uniform anodising of Al around the primary Si phase when compared to conventional DC anodising. Recently, Gudla et al. [40–42] postulated that the homogeneity/uniformity of the anodised Al surfaces is highly affected by the presence, and subsequent incorporation of second phases or intermetallic phases to the anodic layer in fully, partially, or in some cases negligibly oxidised condition. In addition, formation of 'conical asperities' in the anodic layer (entrapped un-anodised Al), due to hindered oxidation of the Al matrix directly below the second phases was also earlier discussed as a factor affecting the uniformity of the anodic layer [20]. Examples of such entrapped Al were initially presented by Walmsley et al. [43], Gudla et al. [44], and more recently by Zhu et al. [45] with the help of Transmission Electron Microscopy (TEM of the anodic film, especially on sections containing incorporated second phases. However, application of high frequency pulse reverse pulse anodising to such Al surfaces was shown to enhance the degree of oxidation of the Al matrix in the vicinity of the second phases, and thus improving the homogeneity of the obtained anodic layers. This was attributed to the anodic pore branching [46–48] during high frequency pulse anodising as was observed using TEM of anodic layer sections. In addition, optical appearance of the anodic layer improved with high frequency pulse anodising when compared to those obtained using conventional DC anodising [42]. The growth rate of the anodic layer was found to increase with an increase in the anodic cycle voltage and with anodising frequency, but was found to be almost independent of the pulse duty cycle within the range of pulse frequencies investigated [47].

Recently, Bononi et al. [33–35] studied pulsed current hard anodising of commercial AA2xxx, AA6xxx, and AA7xxx alloys and reported that an increase of the applied pulse frequency in certain alloys induces a greater difficulty in overcoming critical issues caused by intermetallic phases during anodising in sulfuric acid. Alloys containing critical elements such as Cu in AA2xxx

alloys displayed harder oxides but with higher number of defects in the oxide, while those containing lower amount of Cu like in AA6xxx did not show much increase in number of defects with increasing pulse frequency. In alloys, which do not induce critical elements like Cu that induce parasitic oxygen evolution reactions, the pulse frequency effect is negligible.

Applications for anodised Al surfaces that demand pleasing decorative appearance of the anodised surface usually require a higher purity of the Al alloy being anodised. However, with recent increase in the use of recycled Aluminium alloys for environmental sustainability and cost effectiveness, the quality control of anodised surfaces is increasingly becoming difficult. This is due to the higher degree of heterogeneity in recycled Al alloys that contain a higher number of intermetallic or constituent phase particles, which leads to higher heterogeneity in the electrochemical nature thus altering the anodising behaviour and the decorative finish of the anodised surface [9,49–57]. Various authors have emphasized on the importance of the alloy composition, morphology and microstructure of the Al surface and its effect on the anodising behaviour and optical appearance [58][59]. In general, the optical transparency and quality of an anodic film depends greatly on the micro- and nano-scale morphology of the oxide and the Al substrate morphology and composition. Intermetallics and second phases affect the optical quality of anodised surfaces due to their differences in electrochemical and anodising behaviour, which leads to variations in the structure of the anodized layer or oxide metal interface [60]. Depending on their electrochemical activity with respect to the Al matrix, as described earlier, they are either partially or fully oxidised and incorporated into the anodic film, or are dissolved and lost into the electrolyte leaving behind a void [61]. In view of this, it is interesting to study and understand the effect of high frequency pulse anodising on the structure, properties, and optical quality of the high frequency anodised Al surfaces [62].

The objective of the present work is to investigate high frequency (HF) pulse anodising for aluminium alloys, with the aim of using the technology for decorative purposes. The effect of anodising parameters on the growth rate, optical properties, and anodic layer hardness were investigated. Further, the underlying mechanism behind the optimised growth rate of HF pulse anodising is investigated in comparison with Direct Current (DC) anodising. In order to study the effect of temperature evolution and joule heating during HF anodising, an in-situ temperature measurement setup for the anodising cell is implemented. Use of in-situ temperature measurements has previously been employed to study the temperature close to the anodic barrier layer and how it significantly differs from the temperature of the electrolyte bath [63–67]. Parameters such as Reflected image quality, distinctness of image and gloss values are reported and the observed trends are correlated and explained in terms of the microstructural constituents and their electrochemical behaviour under high frequency pulsed anodising.

2. Experimental

2.1. Alloys and surface preparation

Two different aluminium alloys from alloy families usually applied in decorative anodising are selected for this study; an AA1050, and an AA6401. The AA6401 was obtained in 6 mm thickness as this provides a very flat surface of the alloy critical to optical characterization while allowing for adequate surface processing in order to obtain a reproducible and mirror-like surface. The AA6401 alloy surface was turned in a Hembrug turning machine (Feed=0.08 mm/RPM, Speed=4000 RPM), using several grades of polycrystalline diamond to obtain a flawless surface highly glossy appearance. The turned surfaces were subsequently degreased in a mild alkaline solution (30 g/L, Alficlean™, Alufinish, Germany) for 5 minutes. Desmutting was performed by

immersing in a 100 g/L HNO_3 solution for 30 s followed by demineralised water rinsing. Finally, the samples were cleaned by ultra-sonication in acetone for 15 min and dried in warm air flow.

Having a 6 mm thickness of AA 6401 alloy made it unsuitable for determining the barrier layer temperature during anodising, which in turn could reveal the mechanisms behind HF pulse anodising. To gain precise barrier layer temperature data, it was mandatory to utilise specimens as thin as possible. For this reason another alloy was adopted. AA1050 was thus selected because it is also traditionally used in application where high gloss anodising is necessary and it is commercially available in 0.5 mm thickness. The cold rolled sheet was obtained in a high-gloss state and hence no further processing was performed to the surface. Any residues from the protective foil/adhesive were removed by a degreasing routine similar to that applied for the AA6401 alloy. **Table 1** provides an overview of the chemical composition (in wt.%) of alloy AA6401 and AA1050.

Table 1: Chemical composition of the investigated alloys in wt.%.

	Si	**Fe**	**Cu**	**Mn**	**Mg**	**Cr**	**Zn**	**Ti**	**Al**
AA6401	0.44	0.04	0.12	-	0.39	0.00	0.00	0.01	Balance
AA1050	0.23	0.12	0.02	0.03	0.03	0.01	0.02	0.01	Balance

2.2. High Frequency Pulse Anodising

The AA1050 and AA6401 alloy samples were anodised in a 20 wt.% sulphuric acid bath kept at a constant 18 °C. High frequency square voltage pulses were generated from a function generator (33120A, Agilent). The low powered signal from the function generator was amplified to a high-power signal, using a Class-AB power amplifier that can both source and sink electrical

current. The latter is important for the removal of charges prior to the next pulse cycle. Both voltage and current waveforms were recorded during anodising with the help of an analogue oscilloscope attached to a data acquisitioning system.

The pulse frequency was varied between 100 Hz and 5 kHz. The duty cycle (i.e., the ratio between the anodic cycle duration and the time interval between two subsequent pulses) was varied at 10, 30, 50 and 70%. The offset trials involved a constant upper voltage of 15 V, while lower voltages were varied from -2, 0, 5 and 10 V (i.e. -2 to 15 V, 0 to 15 V, 5 to 15 V, and 10 to 15 V). Reference samples using DC voltage were made in the same anodising cell. The total anodising time was adjusted for each sample to achieve an anodic layer thickness of 10±1 μm. Anodic layer thickness was measured using a Fischer Isoscope gauge. After anodising, the samples were rinsed, sealed and dried. Rinsing was performed in demineralized water for 10 minutes. Hydrothermal sealing of the anodised surfaces was performed by immersing the samples in a water bath maintained at 96 ± 2 °C for a total duration of 25 minutes, followed by drying for 5 minutes in an oven at 70 °C.

2.3. Anodising setup

Anodising was conducted in a custom-built anodising cell based on the flat cell setup that solely anodises one side of the aluminium sheet. This allows direct access to measure the sample temperature from the reverse side. Since the AA1050 sample is just 0.5 mm in thickness (also due to the high thermal conductivity of aluminium), the sample temperature is assumed to be similar to that of the barrier layer temperature. The aluminium sample is mounted vertically up against a rubber gasket that avoids any electrolyte leakage from the anodising cell. The cell is a double walled cell for cooling the electrolyte and to secure constant temperature of the sulphuric acid electrolyte. Air agitation was introduced to secure proper circulation of the electrolyte and thus a

homogenous electrolyte temperature. The circular anodised area was approx. 16 cm^2. A pt100 temperature sensor was attached to the backside of the samples for estimating the barrier layer temperature during anodising. The entire setup is illustrated in Figure 1.

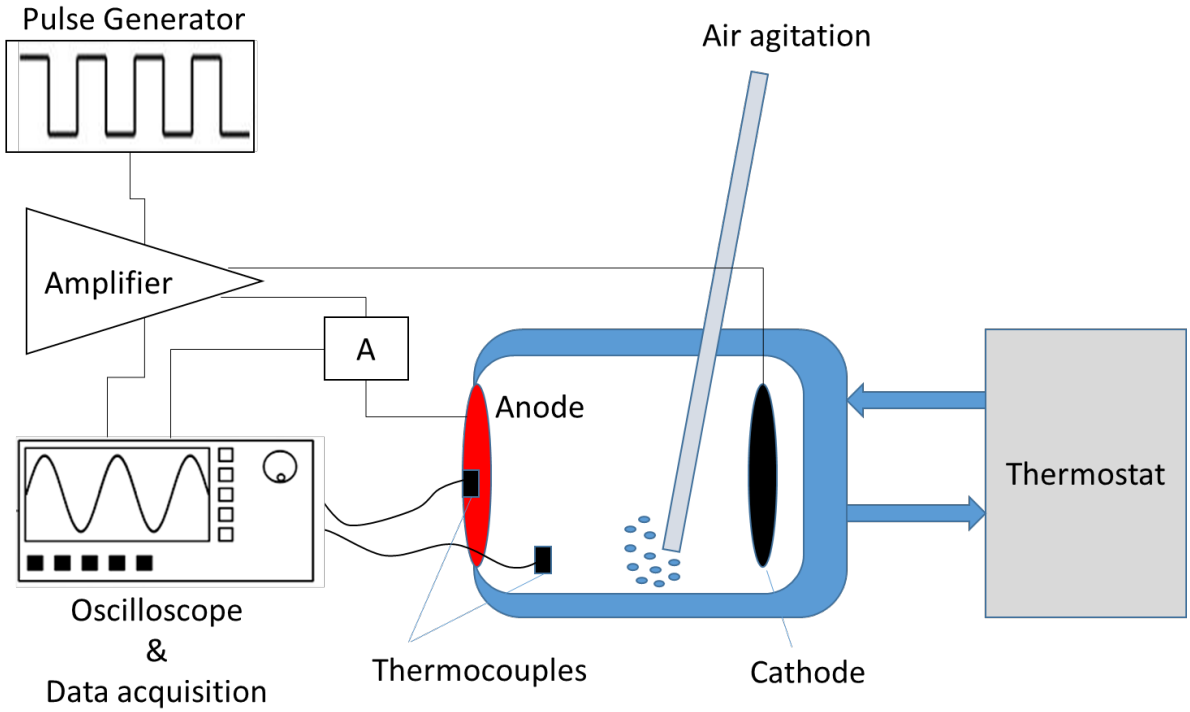

Figure 1: Custom built anodising cell that allows for determining the temperature close to the anodised barrier layer.

2.4. Optical appearance

The surface appearance of the Al alloys after anodising was quantified using a Triple Angle Gloss & DOI meter (Elcometer 408). This equipment captures the reflected light profiles using a light sensitive array consisting of 512 diodes, and outputs values according to ASTM, DIN and ISO standards (ASTM D523, ASTM D2457, ASTM E430, ASTM D5767, DIN 67530, DIN EN ISO 2813, JIS Z 8741, ISO 7668). The gloss values are measured for a 20 degree light incidence angle.

2.5. Microhardness

The micro-Vickers hardness of the anodised surfaces was measured using a Future-Tech FM 700 microhardness tester with a load of 5 g for 5 s. For each sample, a minimum of 10 measurements were performed on the anodic layer cross sections to obtain reliable average hardness values.

3. Results and Discussion

3.1. Voltage-Current response

The voltage-current response during high frequency anodising of the AA6401 is shown in Figure 2. The highly capacitive nature of non-sealed anodic films [68] results in very dramatic current peaks upon sudden changes of voltage. This applies for both changes in the positive and negative direction. Figure 2 is an example of a 1 kHz situation where the voltage is ramped from zero to full voltage (15 V) in few microseconds. This gives rise to a peak current of approx. 30 A/dm^2. As soon as the barrier layer is fully charged, the current drops to a plateau level of approx. 4 A/dm^2; i.e. drastically lower than the peak current, but considerably higher than the current density regime of 1-2 A/dm^2 observed during conventional DC anodising. When the voltage is dropped from 15 V to zero, the barrier layer charges are removed, and a large negative peak current is observed. This negative peak is followed by a plateau of zero ampere, before the next positive cycle is applied. The applied voltage pulse is displayed in **Figure 2**a while the current response is displayed in **Figure 2**b.

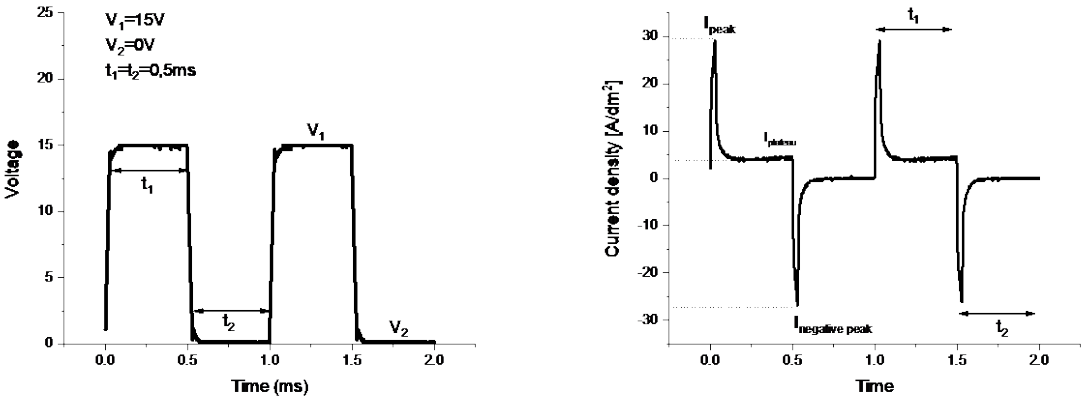

Figure 2: Applied voltage, and measured current response during HF pulse anodising from 0-15 V @ 1 kHz for AA6401.

3.2. Rate of the anodic film growth

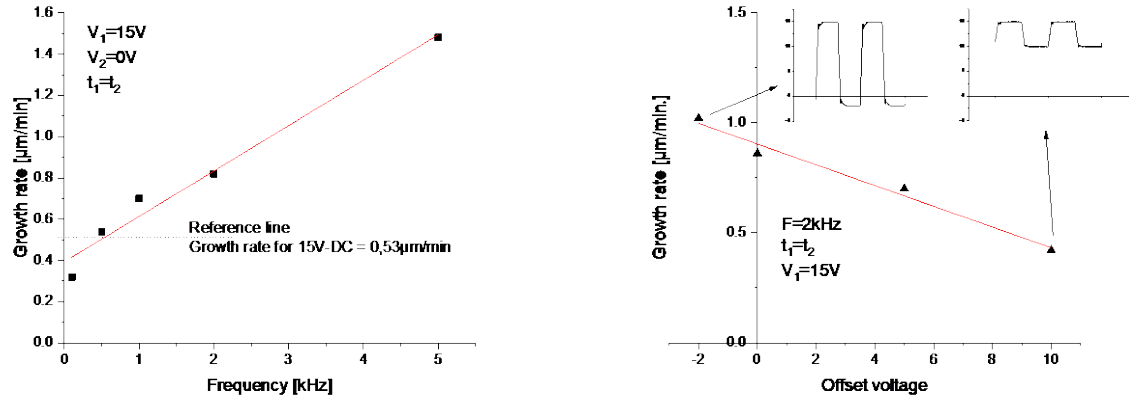

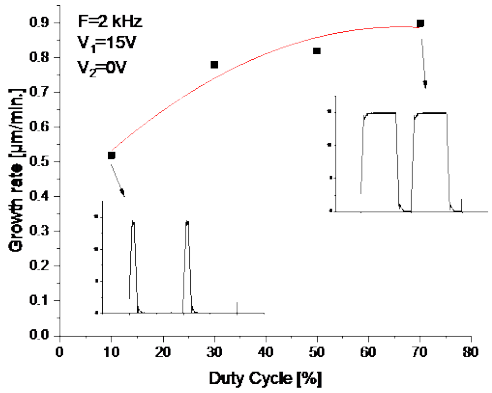

Figure 3: Growth rate of AA6401 during HF pulse anodising as a function of a) pulse frequency, b) anodising voltage offset, and c) pulse duty cycle.

The growth rate of anodic films on the AA6401 alloy was found to be strongly dependent on the anodising conditions, namely the pulse frequency and offset voltage. Figure 3 (a) shows the effect of the pulse frequency on the rate of the anodic film growth. Increasing the pulse frequency from 100 Hz to 5 kHz leads to a significant increase in the growth rate, seemingly with an almost linear relationship across the entire investigated frequency span. The growth rate at 5 kHz was observed to be 1.5 µm/min, which is very high, considering that the growth rate for standard DC-15 V anodising is 0.5 µm/min. As such, the growth rate was tripled when going from DC to 5 kHz. At the other end of the scale, a 100 Hz pulse proved to give a growth rate of 0.3 µm/min, which is lower than conventional DC anodising of similar voltage. A reasonable explanation for this behaviour at lower frequency is the nature of pulse anodising, where 50% of the time (in this case) is in the Off-state and thus not contributing to anodic film growth. However, at higher pulse frequencies in the kHz regime, even though the off time is still 50%, the growth rate is improved considerably. The reason for this behaviour will be discussed in the next section.

Figure 3 (b) shows the dependence of anodic film growth rate on the anodising voltage offset. All anodising conditions were kept constant, only changing the lower voltage level of the

applied pulse cycle. The results suggest that there is a clear trend towards lower growth rate when increasing the lower voltage level. This means that the highest growth rate is achieved when the offset voltage is as low as possible, i.e. as big a difference between upper and lower voltage as possible. Comparing data for -2 V to 15 V with 10 V to 15 V suggests that the growth rate has decreased by more than 50%.

The effect of duty cycle on anodic film growth rate is presented in Figure 3 (c) for an anodising pulse frequency of 2 kHz. There is a general trend towards higher growth rate upon increasing the pulse duty cycle. Especially the gap from 10% to 30% significantly increases the growth rate, whereas the increase from 30% to 50%, and onwards to 70% only has a marginal effect. Most studies in different conditions agree that a level of 70–80% brings the best oxide performances [34,69,70].

3.3. Optical Characterization

It has already been shown that the high frequency pulse anodising yields a very fast anodic film growth. However, for decorative applications, the optical quality like total reflectance, colour, and transparency of the anodised surfaces is of extreme importance in addition to the anodic growth rate. In order to compare the optical properties of anodised surfaces obtained by various DC, and pulse anodising parameters, the anodic layer thickness is maintained constant. Wood [71] explains how the specular reflectivity and image clarity is affected by increasing anodic film thickness, with a dramatic drop for the first few microns, followed by a linear drop as the film thickness increases. To determine if the linear drop has similar slope for high frequency pulse anodising, a series of samples were made with different anodic film thickness. Three different voltages were selected, 10 V, 15 V and 18 V. The film thickness ranges from 5 to 20 μm were investigated as these are within the typical thickness value range used for decorative anodising.

In the top of Figure 4, data is presented for 10 V anodising, showing the drop of surface gloss as the anodic film thickness increases. Conditions for DC, 100 Hz, 1 kHz and 5 kHz anodising are compared, and the results show that the drop in gloss is linear for all anodising conditions. The 10 V data suggests that the pulse anodised samples have marginally better gloss values compared to the DC anodised samples. However, the improvement in gloss upon using pulse anodising is even clearer when increasing the anodising potential. Figure 4 also presents gloss values for samples anodised at 15 V and 18 V. In both the cases, it is quite clear that the gloss values are considerably higher when increasing the pulse frequency. This applies to the entire decorative anodic film thicknesses span of 5-20 μm.

It should be noted that the difference in surface gloss is very evident by evaluating the surfaces with the naked eye. For example, the worst-case sample being 18 V-DC-18 μm, proved to be matt and unattractive from an aesthetical point of view. In strong contrast, the samples anodised at 10 V with low film thickness, all showed mirror-like surface appearance with very good image quality. This is to emphasize that the gloss measurements give a good representation of how the surfaces are perceived by the naked eye.

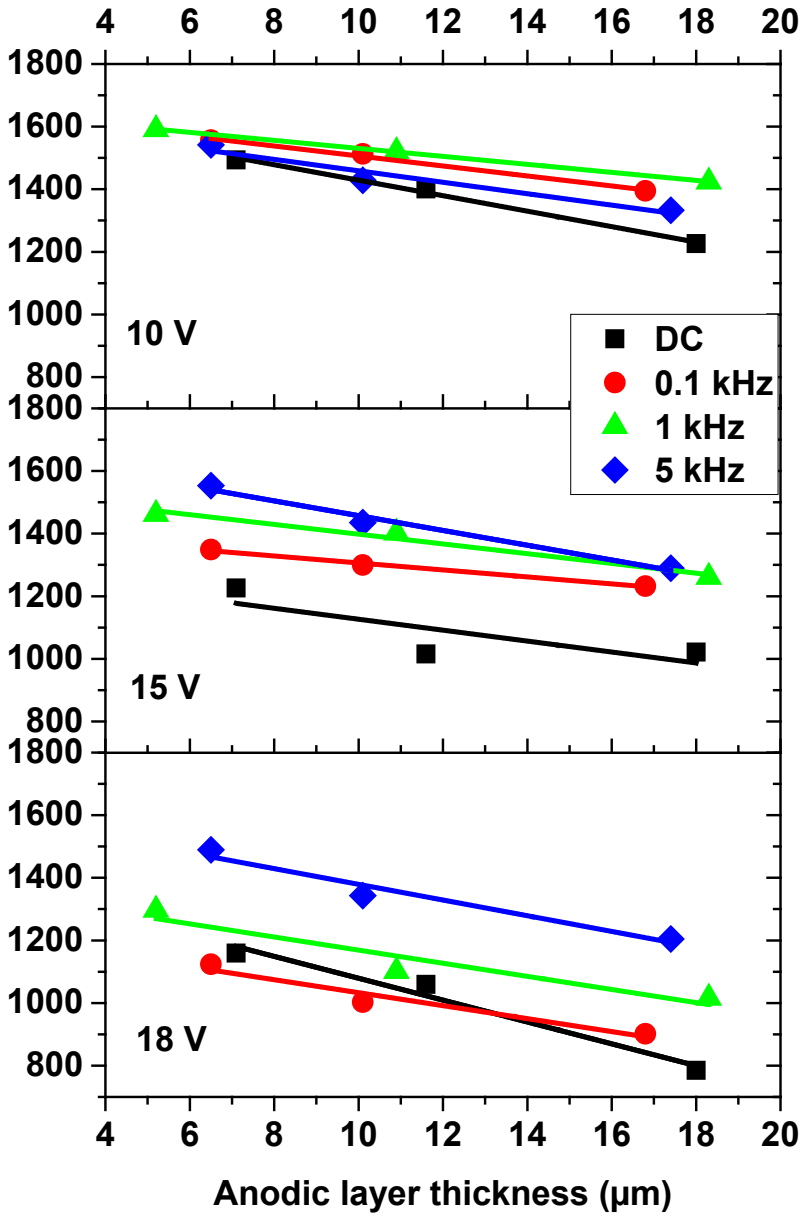

Figure 4: 20° gloss as a function of anodic film thickness and pulse frequency for AA6401.

The presented results that reveal how the anodised appearance becomes better upon increasing pulse frequency, brings out the question of what gloss is affected by. In general, the variables of importance for the aluminium alloy are 1) chemical composition, 2) metallurgical structure, 3) grain size and 4) temper. It is common knowledge that the chemical composition has a huge influence of the anodic appearance, for example with Iron and Silicon having detrimental

effects. In addition, the presence of microscopically visible (0.1 – 0.2 μm or larger) second phase constituents is very detrimental. If the alloy grain size exceeds 90 -100 μm (coarse grained) a bright anodised specimen will reveal a mottled appearance with poor image clarity. This is due to different reaction rates during anodising of grains with different orientation. The effect of alloy temper in the anodising process is to reveal grains of different orientation since they oxidise at difference rates, thus forming a stepped oxide. Hence, fully annealed alloys have lower image clarity than fully hardened alloys [71]. The anodising variables that affect appearance are 1) film thickness, 2) current density, 3) electrolyte temperature, and 4) composition. [20].

As the presented anodising results are based on the same material, film thickness, electrolyte temperature and composition, it is interesting to determine what has changed, since the pulse anodising reveals optimised appearance. The extruded AA6401 alloy which took part in this research was annealed to a point where grains have a size from 100 to 200 μm, making it a rather coarse grained material. This means that the varying reaction rates during anodising of crystals with different orientation can have a detrimental effect on the optical appearance. As such, it is highly plausible that the kinetics of crystals with different orientation is altered when going from DC to pulse anodising mode. It is likely that crystals of different orientation have larger kinetic differences at DC than they do when moving up in frequency. This hypothesis is not verified here, but will be part of future trials.

3.4. Hardness measurements

As high frequency pulse anodising yields a porous oxide with complex branched structure [46][47], it was of interest to determine if the resulting oxide has sufficient hardness. This is important for industrial applications where scratch and wear resistance is of paramount importance. Samples with a 10 μm oxide thickness were vertically positioned in an epoxy mount, followed by

grinding and polishing. This allowed for micro Vickers hardness characterization in the cross sectional direction. Figure 5 shows average values for 10 individual measurements. These results typically range between 400 and 500 HV with no clear indication that pulse anodising should be any better or worse than conventional DC anodising. This could suggest that the oxide branching during high frequency pulse anodising does not compromise the mechanical strength. This is in good agreement with data from Juhl et al. [38] who studied pulse anodising of extruded and cast Al alloys, and investigated how pulsing conditions affected the oxide hardness.

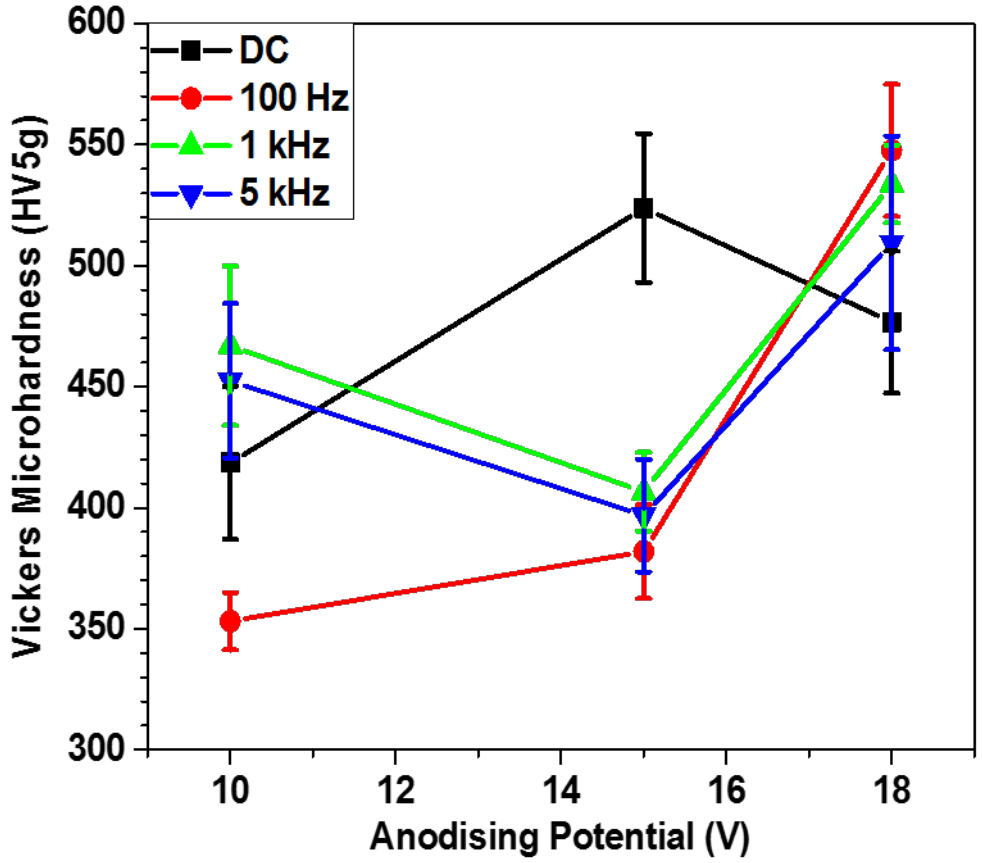

Figure 5: Vickers micro-hardness of anodic oxides anodised at different conditions. 5 g load for 5 s.

3.5. Mechanism behind HF Pulse anodising

Improved kinetics during pulse anodising are often explained by the so-called *Recovery Effect*, which was investigated by Takahashi et al. [72]. In short, the recovery effect deals with a thinning of the anodic barrier layer during the pulse off-cycle due to chemical dissolution by the electrolyte [73][74]. Thinning the barrier layer means that the electric field across the barrier film increases once the on-cycle is applied, giving rise to increased rate of ion transport through the barrier oxide. Gudla et al. [62] reported how high frequency switching improves the anodising kinetics considerably, however, the underlying mechanism for better kinetics was not investigated. The hypothesis is that the cathodic cycle or the off cycle during the pulse anodising process allows for the dissolution and mechanical weakening of the formed anodic oxide at the substrate interface thus increasing the anodising rate in the subsequent anodic cycle. However, open circuit anodic barrier layer dissolution studies show that the dissolution of the barrier oxide is not considerable within the off time intervals (100 μs – 5000 μs) associated with high frequency pulse anodising [72–76] thus opening the discussion for underlying mechanism for observed improved anodising kinetics under high frequency pulse anodising, mainly the effects of temperature evolution.

Figure 6 presents data that compare the barrier layer temperature and the anodic film growth rate. In all the presented cases, there is a clear relationship between the two parameters, suggesting that a high barrier layer temperature always results in a high film growth rate. The barrier layer temperature reaches levels much higher than that of the bulk of the anodising electrolyte, which was maintained stable at 18 °C. For example, an aggressive anodising signal of 15 V-5 kHz gives rise to a barrier layer temperature of approximately 27 °C, which is almost 10 degrees higher than the surrounding electrolyte. Figure 6 (b) shows how a duty cycle of just 10% punishes the film growth rate with a low value of ~0.5 μm/min. This growth rate increases to ~0.8

µm/min for 30% and 50% duty cycle, and reaches 0.9 µm/min at 70%. These findings suggest that the off-period of a pulse cycle does not need an extensive duration in order to provide good anodising kinetics.

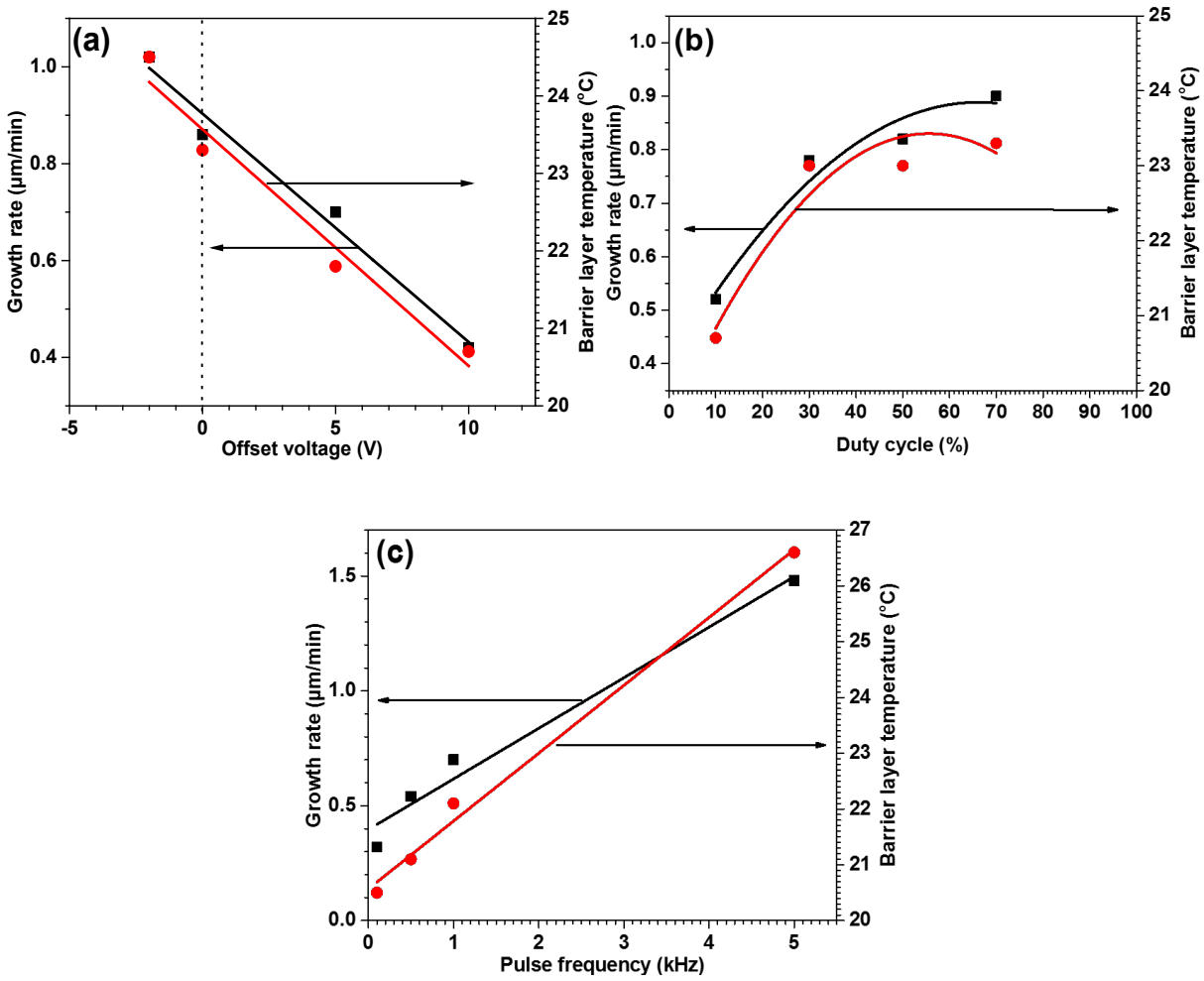

Figure 6: Barrier layer temperature & anodic film growth rate for AA1050 as a function of a) offset potential, @ 2 kHz, 50% duty cycle b) pulse duty cycle, @ 2 kHz, 0-15 V, and c) pulse frequency, @ 0-15 V, 50% duty cycle.

The increase in the local temperature at the barrier layer can be explained by the dielectric losses within the anodic alumina barrier layer. Dielectric loss is defined as the loss of energy in the form of heat by a dielectric material under the action of an alternating voltage. Anodised alumina is

also used for electric storage capacitors [77], where dielectric loss is a very well-known phenomena. For this application, it is widely recognized that increased frequency yields high temperature of the capacitor due to dielectric losses. As such, it is valid to argue that the alternating voltage during high frequency pulse anodising causes the alumina barrier layer to heat up due to dielectric losses, and that increased temperature will have a positive effect on the ion flux through the barrier layer. However, the results in Figure 6 do not provide a clear indication of the dominant parameter i.e., if the barrier layer temperature controls growth rate, or, in fact, a high growth rate results in a high barrier layer temperature. In order to investigate this in more detail, another study was performed where the power consumption and the barrier layer were logged as a function of anodising time. Two different scenarios were examined:

1. Standard pulse anodising, with monitoring of power consumption and barrier layer temperature. This is denoted as "Sample 1" in Figure 7.
2. Same conditions as 1) but with a prior aggressive pulse anodising that causes the barrier layer to heat up to a higher level. This is denoted as "Sample 2" in Figure 7.

Both the AA1050 samples were anodised for a total duration of 10 minutes and data was logged every 20 s. The power consumption for Sample 1 reaches steady state within the first 100 s of anodising, whereas barrier layer temperature lags behind and requires approx. 200 s before reaching a stable plateau level. Sample 2 is first anodised with an aggressive pulse anodising signal, which causes the barrier layer temperature to reach approx. 29 °C. The anodising signal is subsequently dropped to similar settings as that of Sample 1, which makes both power consumption and barrier temperature drop to significantly lower levels. The interesting observation is the speed at which both parameters decrease. Power consumption decreases almost instantly, whereas barrier layer temperature takes a while to reach the new steady state level. Thus, both Sample 1 and Sample 2 suggest that barrier layer temperature does NOT dictate growth rate, rather, the data suggests that

growth rate dictates barrier layer temperature. As such, dielectric losses within the anodic alumina barrier layer do not seem to play a significant role in high frequency pulse anodising kinetics – at least not within the investigated the frequency range of 100 Hz to 5 kHz.

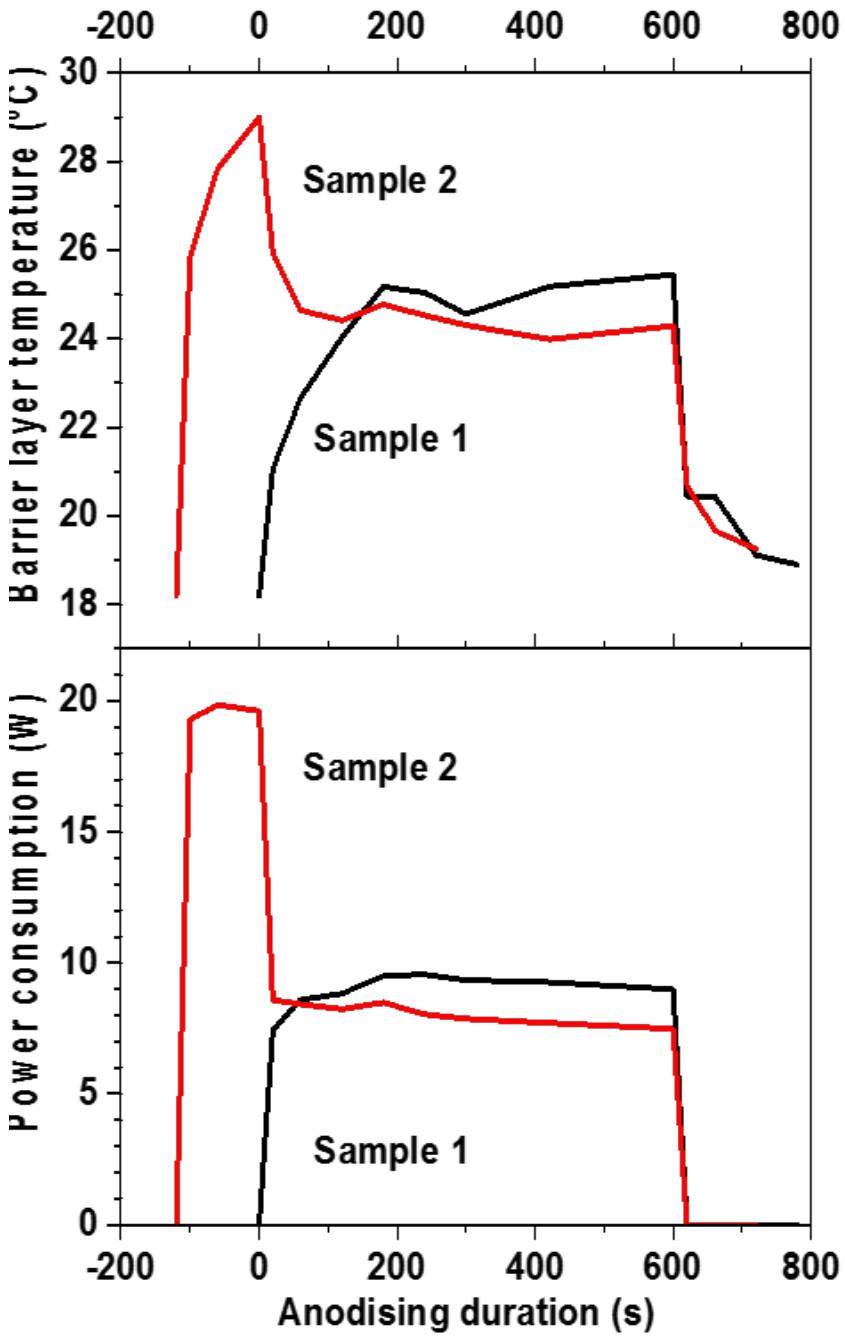

Figure 7: Power consumption and barrier layer temperature as a function of time.

3.6. Gouy-Chapman and Helmholtz Layers

Tian et al. [78] describe how Gouy-Chapman and Helmholtz layers can control the ion transport through the anodic barrier layer, and hence the film growth rate. Indeed, if these layers are present and introduce a significant resistance towards the chemical reactions, these can explain that high frequency pulse anodising yields different ion transport kinetics compared to conventional direct current anodising.

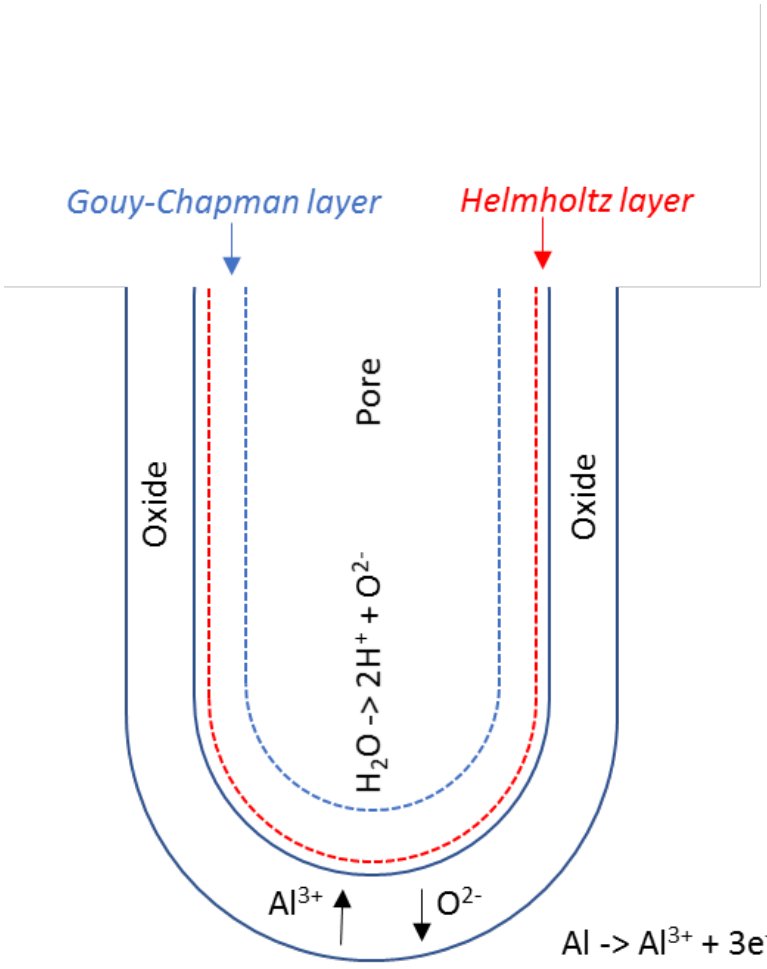

Figure 8: Gouy-Chapman and Helmholtz Layers.

To test this hypothesis, another setup was constructed, where the peak currents during the initiation of the on-cycle were examined. If the barrier layer were thinner upon high frequency pulse

anodising, this would be observed as a higher peak current compared to low frequency anodising. Studying these peak currents requires a power generator that can deliver power ultra-fast. As such, the only viable solution was to use large storage capacitors that deliver power almost instantaneously. These capacitors were switched on and off using Sold State Relays (SSRs). The upper frequency was limited to 2.5 kHz due to the restrictions of the relays. A series of frequencies ranging all the way from 10 Hz up to 2.5 kHz were tested, while recording the current response signal with a high speed data acquisition system.

The current response profiles presented in Figure 9 show almost identical characteristics but with a slight increase of peak values with increasing pulse frequency. The increase of peak current from 100 Hz to 2.5 kHz corresponds to 4.4%. In addition, the plateau level that follows the current peak is observed to increase upon increasing pulse frequency. In other words, it is the combined effect of increased peak and plateau current that results in an overall increased power consumption upon increasing anodising pulse frequency.

The peak values extracted and presented in Figure 10 suggest that a logarithmic trend exists between applied anodising pulse frequencies and observed anodising peak current. This indicates a decreasing thickness of Gouy-Chapman and Helmholtz layers upon increasing the anodising potential pulse frequency.

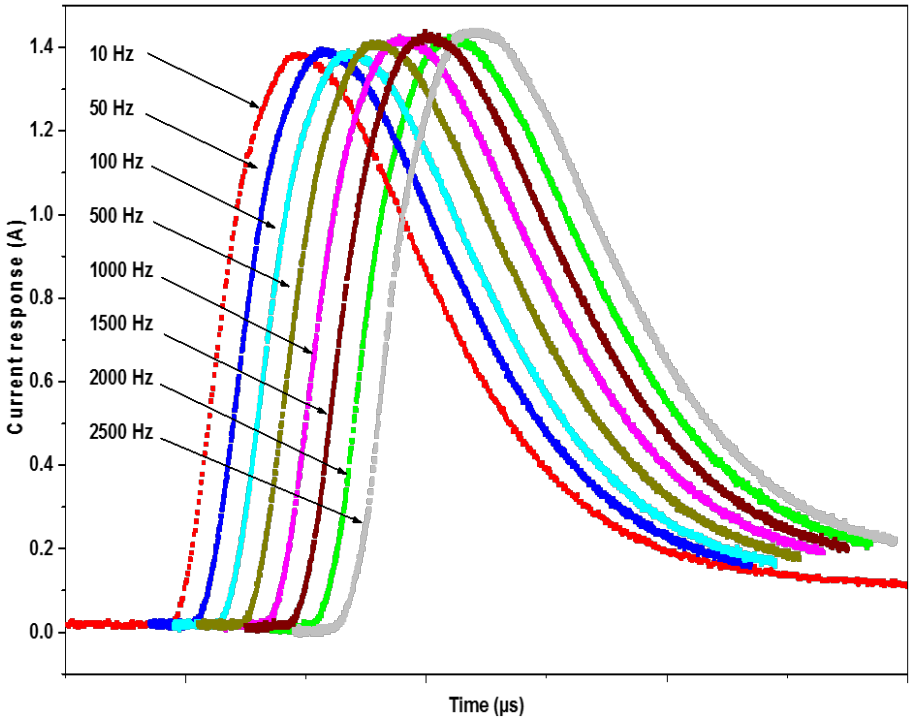

Figure 9: Peak current profiles for different pulse anodising frequencies.

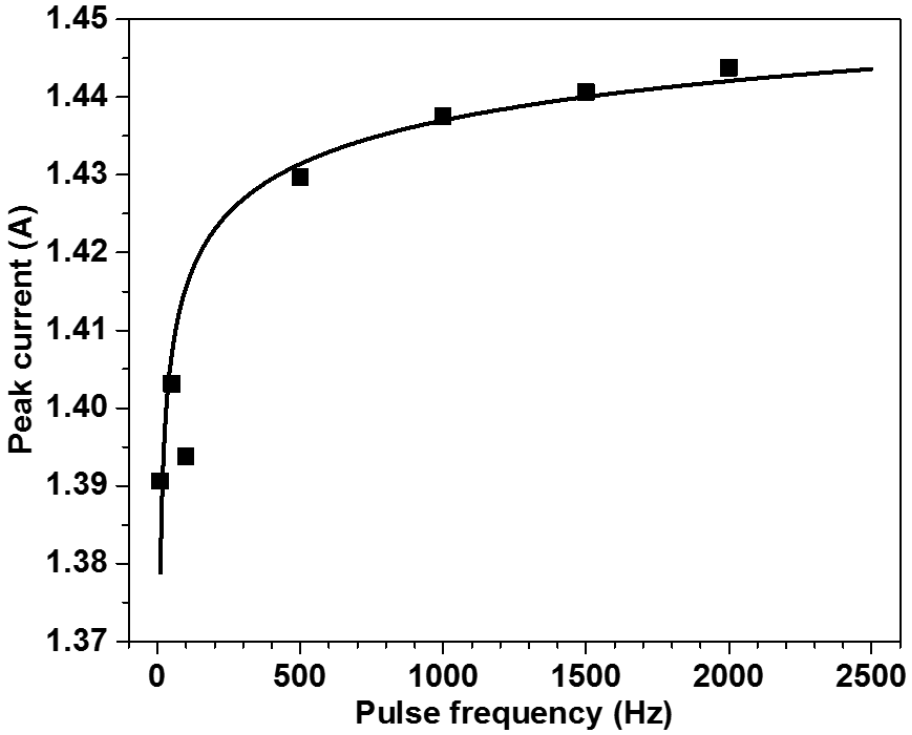

Figure 10: Anodising peak current vs. applied pulse frequency for AA1050.

The observations presented above reveal that the anodising kinetics and the optical appearance are improved when moving from direct current anodising to high frequency pulse anodising mode. This is in close resemblance to the observations that are made for electrodeposition of certain metals where it is well documented that pulse electrodeposition is associated with advantages such as significant improvement in surface properties, higher deposition rates, reduction in porosity, better corrosion resistance, less porosity, reduced grain size and lower surface roughness [79] [80]. Maharana et al. [80] concludes that surface roughness decreases during increasing frequency upon electrodeposition of Cu-SiO_2 coatings. This is explained by a greater number of nucleation sites upon using pulse mode compared to direct current, which in turn leads to a smoother film with a lower R_a value. Generally, this is explained under the topic of electro-crystallization with instantaneous and progressive growth mechanisms [81]. However, anodising of Aluminium differs from metal deposition in several ways. Growth of anodic films requires the

migration of ionic species, and only occurs in the presence of large impressed fields of the order of 10^6 V/cm [81]. This type of electrode process is referred to as field-assisted migration. The mechanism of pore growth in Aluminium anodising has been continuously investigated for the past few decades and is still under debate. In terms of driving force for pore growth, as well as the self-organization of pores towards ordering, two types of models have been proposed; one based on electrical field as the driving force, and the other on mechanical stress as the driving force. For the former model, Hoar and Mott first suggested that under the high electrical field over the barrier layer, hopping of ions takes place by means of jumping from one interstitial position to another, following the Cabrera-Mott equation. The rate-determining step has previously been reported to be related to the bulk oxide [82], however, more recent research has shown that an increase in acid concentration of the electrolyte, can influence the anodising process significantly, such as increase of pore diameter [83], current density [84] and oxide growth rate [85]. These findings suggest that the rate-determining step is in the oxide/electrolyte interface, rather than the bulk of the oxide itself [86]. As such, these observations go well with the high frequency pulse anodising studies mentioned here, where it has been shown that an increase in pulse frequency yields an altered condition at the barrier layer. Increasing pulse frequency gives increasing peak current amplitude, which suggests that the electrochemical impedance is lowered.

4. Conclusions

High frequency pulse anodising of aluminium alloy AA6401 was investigated to understand the effect of anodising parameters on growth kinetics and optical appearance of the anodised surface. The conclusions are:

1. Oxide growth rate is highly dependent on both pulse frequency and offset potential level. Increasing frequency yields an almost linear increase of growth rate. Growth rates up to 3

times higher compared to conventional DC anodising are observed. Increasing offset voltage has a negative impact on growth rate

2. Oxide growth rate is slightly affected by pulse duty cycle. An optimum seems to exist at 70%, but 50% and 30% data are not considerably lower. Decreasing duty cycle to 10% will punish the kinetics drastically.
3. Anodising pulse potential, and pulse frequency have paramount influence of the measured anodic surface gloss. In general, lower voltages favour a glossy appearance. Increasing pulse frequency improves the gloss considerably, especially when combined with a high anodising voltage.

Next, an effort was made to determine why high frequency pulse anodising yields improved kinetics compared to traditional DC anodising. The main conclusions are:

4. A very clear correlation exists between the barrier layer temperature and the film growth rate.
5. Dielectric losses of the alumina barrier layer are NOT controlling overall process kinetics. Test results suggest that Gouy-Chapman and Helmholtz Layers become thinner upon increasing frequency, and that this phenomenon is contributing to an increased oxide growth rate.

Acknowledgements

The authors would like to thank Innovation Fund Denmark for their financial support of Industrial PhD Flemming Jensen (Grant No. 5016-00128B).

References

[1] J.C. Williams, E.A. Starke, Progress in structural materials for aerospace systems, Acta Mater. 51 (2003) 5775–5799. doi:10.1016/j.actamat.2003.08.023.

[2] E.A. Starke Jr, J.T. Staley, 24 - Application of modern aluminium alloys to aircraft, in: R.B.T.-F. of A.M. Lumley (Ed.), Fundam. Alum. Metall., Woodhead Publishing, 2011: pp. 747–783. doi:http://dx.doi.org/10.1533/9780857090256.3.747.

[3] A. Heinz, A. Haszler, C. Keidel, S. Moldenhauer, R. Benedictus, W.S. Miller, Recent development in aluminium alloys for aerospace applications, Mater. Sci. Eng. A. 280 (2000) 102–107. doi:10.1016/S0921-5093(99)00674-7.

[4] W.S. Miller, L. Zhuang, J. Bottema, A.J. Wittebrood, P. De Smet, A. Haszler, A. Vieregge, Recent development in aluminium alloys for the automotive industry, Mater. Sci. Eng. A. 280 (2000) 37–49. doi:10.1016/S0921-5093(99)00653-X.

[5] K. Bordo, V.C. Gudla, L. Peguet, A. Afseth, R. Ambat, Electrochemical profiling of multi-clad aluminium sheets used in automotive heat exchangers, Corros. Sci. 131 (2018) 28–37. doi:10.1016/j.corsci.2017.11.011.

[6] C. Vargel, Corrosion of Aluminium, Elsevier B.V., 2004. doi:10.1016/B978-0-08-044495-6.X5000-9.

[7] Z. Szklarska-Smialowska, Pitting corrosion of aluminum, Corros. Sci. 41 (1999) 1743–1767. doi:10.1016/S0010-938X(99)00012-8.

[8] V. Kevorkijan, The recycle of wrought aluminum alloys in Europe, Jom. 54 (2002) 38–41. doi:10.1007/BF02701072.

[9] J. Cui, H.J. Roven, Recycling of automotive aluminum, Trans. Nonferrous Met. Soc. China (English Ed. 20 (2010) 2057–2063. doi:10.1016/S1003-6326(09)60417-9.

[10] G. Wallace, 4 - Production of secondary aluminium, in: R.B.T.-F. of A.M. Lumley (Ed.), Woodhead Publ. Ser. Met. Surf. Eng., Woodhead Publishing, 2011: pp. 70–82. doi:http://dx.doi.org/10.1533/9780857090256.1.70.

[11] D. Dispinar, a Kvithyld, a Nordmark, Quality assesment of recycled aluminium, in: TMS Light Met., SINTEF Materials and Chemistry, Trondheim, N-7465, Norway, 2011: pp. 731–735. http://www.scopus.com/inward/record.url?eid=2-s2.0-79955155793&partnerID=40&md5=099efb2d228370a68ed6f404493717ee.

[12] Organisation of European Aluminium Refiners and Remelters (OEA), European Aluminium Association (EAA), Aluminium Recycling in Europe, Eur. Alum. Assoc. Brussels. (2006) 52. http://scholar.google.com/scholar?hl=en&btnG=Search&q=intitle:Aluminium+recycling:+the+road+to+high+quality+products#0 (accessed May 21, 2014).

[13] S.K. Das, Designing Aluminium Alloys for a Recycling Friendly World, Mater. Sci. Forum. 519–521 (2006) 1239–1244. doi:10.4028/www.scientific.net/MSF.519-521.1239.

[14] M. Mahfoud, D. Emadi, Aluminum Recycling - Challenges and Opportunities, Adv. Mater. Res. 83–86 (2009) 571–578. doi:10.4028/www.scientific.net/AMR.83-86.571.

[15] G.. Thompson, Porous anodic alumina: fabrication, characterization and applications, Thin Solid Films. 297 (1997) 192–201. doi:10.1016/S0040-6090(96)09440-0.

[16] S.T. Abrahami, J.M.M. de Kok, V.C. Gudla, R. Ambat, H. Terryn, J.M.C. Mol, Interface strength and degradation of adhesively bonded porous aluminum oxides, Npj Mater. Degrad. 1 (2017) 8. doi:10.1038/s41529-017-0007-0.

[17] R.U. Din, V.C. Gudla, M.S. Jellesen, R. Ambat, Accelerated growth of oxide film on aluminium alloys under steam: Part I: Effects of alloy chemistry and steam vapour pressure on microstructure, Surf. Coatings Technol. 276 (2015) 77–88. doi:10.1016/j.surfcoat.2015.06.059.

[18] I. Schoukens, F. Cavezza, J. Cerezo, V. Vandenberghe, V.C. Gudla, R. Ambat, Influence of de-icing salt chemistry on the corrosion behavior of AA6016, Mater. Corros. 69 (2018) 881–887. doi:10.1002/maco.201709907.

[19] R.U. Din, V.C. Gudla, M.S. Jellesen, R. Ambat, Microstructure and corrosion performance of steam-based conversion coatings produced in the presence of TiO2particles on aluminium alloys, Surf. Coatings Technol. 296 (2016) 1–12. doi:10.1016/j.surfcoat.2016.03.093.

[20] P.G. Sheasby, R. Pinner, S. Wernick, The Surface Treatment and Finishing of Aluminium and Its Alloys, 6th ed., ASM International; Finishing Publications, 2001.

[21] C.A. Grubbs, Anodizing of aluminum, Met. Finish. 105 (2007) 397–412. doi:10.1016/S0026-0576(07)80359-X.

[22] C.A. Grubbs, Decorative and architectural anodizing, Met. Finish. 93 (1995) 449–459. doi:10.1016/0026-0576(95)93394-H.

[23] P. Møller, L.P. Nielsen, Advanced surface technology : a holistic view on the extensive and intertwined world of applied surface engineering, NASF, 2013.

[24] J.W. Diggle, T.C. Downie, C.W. Goulding, Anodic oxide films on aluminum, Chem. Rev. 69 (1969) 365–405. doi:10.1021/cr60259a005.

[25] G.E. Thompson, G.C. Wood, Porous anodic film formation on aluminium, Nature. 290 (1981) 230–232. doi:10.1038/290230a0.

[26] G. Thompson, R.C. Furneaux, G.C. Wood, J.A. Richardson, J.S. Goode, Nucleation and

growth of porous anodic films on aluminium, Nature. 272 (1978) 433–435. doi:10.1038/272433a0.

[27] N. Tabrizian, H.N. Hansen, P.E. Hansen, R. Ambat, P. Møller, Influence of annealing and deformation on optical properties of ultra precision diamond turned and anodized 6060 aluminium alloy, Surf. Coatings Technol. 204 (2010) 2632–2638. doi:10.1016/j.surfcoat.2010.02.002.

[28] A.K. Mukhopadhyay, A.K. Sharma, Influence of Fe-bearing particles and nature of electrolyte on the hard anodizing behaviour of AA 7075 extrusion products, Surf. Coatings Technol. 92 (1997) 212–220. doi:10.1016/S0257-8972(97)00102-3.

[29] M. Saenz de Miera, M. Curioni, P. Skeldon, G.E. Thompson, The behaviour of second phase particles during anodizing of aluminium alloys, Corros. Sci. 52 (2010) 2489–2497. doi:10.1016/j.corsci.2010.03.029.

[30] M. Aggerbeck, S. Canulescu, K. Dirscherl, V.E. Johansen, S. Engberg, J. Schou, R. Ambat, Appearance of anodised aluminium: Effect of alloy composition and prior surface finish, Surf. Coatings Technol. 254 (2014) 28–41. doi:10.1016/j.surfcoat.2014.05.047.

[31] H. Habazaki, K. Shimizu, P. Skeldon, G.E. Thompson, G.C. Wood, X. Zhou, Effects of alloying elements in anodizing of aluminium, Trans. Inst. Met. Finish. 75 (1997) 18–23.

[32] H. Habazaki, K. Shimizu, P. Skeldon, G.E. Thompson, G.C. Wood, The incorporation of metal ions into anodic films on aluminium alloys, Philos. Mag. B-PHYSICS Condens. MATTER Stat. Mech. Electron. Opt. Magn. Prop. 73 (1996) 445–460.

[33] M. Bononi, R. Giovanardi, A. Bozza, Pulsed current hard anodizing of heat treated aluminum alloys: Frequency and current amplitude influence, Surf. Coatings Technol. (2016). doi:10.1016/j.surfcoat.2016.10.025.

[34] M. Bononi, M. Conte, R. Giovanardi, A. Bozza, Hard anodizing of AA2099-T8 aluminum-lithium-copper alloy: Influence of electric cycle, electrolytic bath composition and temperature, Surf. Coatings Technol. 325 (2017) 627–635. doi:10.1016/j.surfcoat.2017.07.028.

[35] M. Bononi, R. Giovanardi, A. Bozza, P. Mattioli, Pulsed current effect on hard anodizing process of 2024-T3 aluminium alloy, Surf. Coatings Technol. 289 (2016) 110–117. doi:10.1016/j.surfcoat.2016.01.056.

[36] M. Sieber, R. Morgenstern, T. Lampke, Anodic oxidation of the AlCu4Mg1 aluminium alloy with dynamic current control, Surf. Coatings Technol. 302 (2016) 515–522.

doi:10.1016/j.surfcoat.2016.06.043.

[37] K. Yokoyama, H. Konno, H. Takahashi, M. Nagayama, Advantages of Pulse Anodizing, Plat. Surf. Finish. 69 (1982) 62–65. http://www.scopus.com/inward/record.url?eid=2-s2.0-0020155469&partnerID=tZOtx3y1.

[38] A. Deacon Juhl, Pulse anodising of extruded and cast aluminium alloys, Technical University of Denmark, 1999.

[39] T. Yamamoto, H. Tanaka, M. Fujita, H. Asoh, S. Ono, Effect of high-frequency switching electrolysis on film thickness uniformity of anodic oxide film formed on AC8A Aluminum alloy, J. Japan Inst. Light Met. 60 (2010) 602–607. doi:10.2464/jilm.60.602.

[40] V.C. Gudla, S. Canulescu, R. Shabadi, K. Rechendorff, K. Dirscherl, R. Ambat, Structure of anodized Al-Zr sputter deposited coatings and effect on optical appearance, Appl. Surf. Sci. 317 (2014) 1113–1124. doi:10.1016/j.apsusc.2014.09.037.

[41] V.C. Gudla, S. Canulescu, R. Shabadi, K. Rechendorff, J. Schou, R. Ambat, Anodization and Optical Appearance of Sputter Deposited Al-Zr Coatings, in: J. Grandfield, TMS (Eds.), Light Met. 2014, John Wiley & Sons, Inc., 2014: pp. 369–373. doi:10.1002/9781118888438.ch63.

[42] M. Aggerbeck, A. Junker-Holst, D.V. Nielsen, V.C. Gudla, R. Ambat, Anodisation of sputter deposited aluminium-titanium coatings: Effect of microstructure on optical characteristics, Surf. Coatings Technol. 254 (2014) 138–144. doi:10.1016/j.surfcoat.2014.05.073.

[43] J.C. Walmsley, C.J. Simensen, A. Bjørgum, F. Lapique, K. Redford, The Structure and Impurities of Hard DC Anodic Layers on AA6060 Aluminium Alloy, J. Adhes. 84 (2008) 543–561. doi:10.1080/00218460802161590.

[44] V.C. Gudla, F. Jensen, A. Simar, R. Shabadi, R. Ambat, Friction stir processed Al–TiO2 surface composites: Anodising behaviour and optical appearance, Appl. Surf. Sci. 324 (2015) 554–562. doi:http://dx.doi.org/10.1016/j.apsusc.2014.10.151.

[45] B. Zhu, S. Seifeddine, P.O.Å. Persson, A.E.W. Jarfors, P. Leisner, C. Zanella, A study of formation and growth of the anodised surface layer on cast Al-Si alloys based on different analytical techniques, Mater. Des. 101 (2016) 254–262. doi:10.1016/j.matdes.2016.04.013.

[46] V.C. Gudla, F. Jensen, K. Bordo, A. Simar, R. Ambat, Effect of High Frequency Pulsing on the Interfacial Structure of Anodized Aluminium-TiO2, J. Electrochem. Soc. 162 (2015) C303–C310. doi:10.1149/2.0311507jes.

[47] V.C. Gudla, K. Bordo, F. Jensen, S. Canulescu, S. Yuksel, A. Simar, R. Ambat, High

frequency anodising of aluminium-TiO<inf>2</inf> surface composites: Anodising behaviour and optical appearance, Surf. Coatings Technol. 277 (2015) 67–73. doi:10.1016/j.surfcoat.2015.07.035.

[48] V.C. Gudla, K. Bordo, S. Engberg, K. Rechendorff, R. Ambat, High frequency pulse anodising of magnetron sputtered Al-Zr and Al-Ti Coatings, Mater. Des. 95 (2016) 340–347. doi:10.1016/j.matdes.2016.01.091.

[49] Y. Ma, X. Zhou, G.E. Thompson, J.O. Nilsson, M. Gustavsson, A. Crispin, Anodizing of AA6063 aluminium alloy profiles: Generation of dark appearance, Surf. Interface Anal. 45 (2013) 1479–1484. doi:10.1002/sia.5219.

[50] G. Vander Voort, B. Suárez Peña, J. Asensio Lozano, Microstructure Investigations of Streak Formation in 6063 Aluminum Extrusions by Optical Metallographic Techniques, Microsc. Microanal. 19 (2013) 276–284. doi:10.1017/S143192761300010X.

[51] H. Zhu, T. Wei, M.J. Couper, A.K. Dahle, Effect of Fe-rich particles on the formation of die streaks on anodized aluminum extrusions, Jom. 64 (2012) 337–345. doi:10.1007/s11837-012-0252-1.

[52] H. Zhu, T. Wei, M.J. Couper, A.K. Dahle, Effect of extrusion profile on surface microstructure and appearance of aluminum extrusions with different Fe contents, JOM. 65 (2013) 618–624. doi:10.1007/s11837-013-0581-8.

[53] H. Zhu, M.J. Couper, A.K. Dahle, Effect of process variables on the formation of streak defects on anodized aluminum extrusions: An overview, High Temp. Mater. Process. 31 (2012) 105–111. doi:10.1515/htmp-2012-0024.

[54] H. Zhu, X. Zhang, M.J. Couper, A.K. Dahle, Effect of initial microstructure on surface appearance of anodized aluminum extrusions, Metall. Mater. Trans. A Phys. Metall. Mater. Sci. 40 (2009) 3264–3275. doi:10.1007/s11661-009-9976-0.

[55] J.B. Hess, Physical metallurgy of recycling wrought aluminum alloys, Metall. Trans. A. 14 (1983) 323–327. doi:10.1007/BF02644210.

[56] Y. Chino, M. Mabuchi, S. Otsuka, K. Shimojima, H. Hosokawa, Y. Yamada, C. Wen, H. Iwasaki, Corrosion and mechanical properties of recycled 5083 aluminum alloy by solid state recycling, Mater. Trans. 44 (2003) 1284–1289. doi:10.2320/matertrans.44.1284.

[57] Y. Ma, X. Zhou, J. Wang, G.E. Thompson, W. Huang, J.-O. Nilsson, M. Gustavsson, A. Crispin, Discoloration of Anodized AA6063 Aluminum Alloy, J. Electrochem. Soc. 161 (2014) C312–C320. doi:10.1149/2.065406jes.

[58] E. Senel, M. Hallenstvet, Effect of Alloying Elements on the Colour Development of Anodised Al-Mg-Si Alloys, Mater. Sci. Forum. 794–796 (2014) 247–252. doi:10.4028/www.scientific.net/MSF.794-796.247.

[59] L.F. Mendes, A.S. Moraes, J.S. Santos, F.L. Leite, F. Trivinho-Strixino, Investigation of roughness and specular quality of commercial aluminum (6061 alloy) for fabrication of nanoporous anodic alumina films, Surf. Coatings Technol. 310 (2017) 199–206. doi:10.1016/j.surfcoat.2016.12.068.

[60] H. Zhu, X. Zhang, M.J. Couper, A.K. Dahle, Effect of primary intermetallic particles on surface microstructure and appearance of aluminium extrusions, Mater. Chem. Phys. 113 (2009) 401–406. doi:10.1016/j.matchemphys.2008.07.109.

[61] G. Gaustad, E. Olivetti, R. Kirchain, Improving aluminum recycling: A survey of sorting and impurity removal technologies, Resour. Conserv. Recycl. 58 (2012) 79–87. doi:10.1016/j.resconrec.2011.10.010.

[62] V.C. Gudla, Optically Designed Anodised Aluminium Surfaces: Microstructural and Electrochemical Aspects, Technical University of Denmark, 2015.

[63] T. Aerts, T. Dimogerontakis, I. De Graeve, J. Fransaer, H. Terryn, Influence of the anodizing temperature on the porosity and the mechanical properties of the porous anodic oxide film, Surf. Coatings Technol. 201 (2007) 7310–7317. doi:10.1016/j.surfcoat.2007.01.044.

[64] P. Chowdhury, A.N. Thomas, M. Sharma, H.C. Barshilia, An approach for in situ measurement of anode temperature during the growth of self-ordered nanoporous anodic alumina thin films: Influence of Joule heating on pore microstructure, Electrochim. Acta. 115 (2014) 657–664. doi:10.1016/j.electacta.2013.10.178.

[65] G.C. TU, I.T. CHEN, K. SHIMIZU, The temperature rise and burning for high rate anodizing of aluminum in oxalic acid., J. Japan Inst. Light Met. 40 (1990) 382–389. doi:10.2464/jilm.40.382.

[66] I. De Graeve, H. Terryn, G.E. Thompson, Influence of Local Heat Development on Film Thickness for Anodizing Aluminum in Sulfuric Acid, J. Electrochem. Soc. 150 (2003) B158. doi:10.1149/1.1560639.

[67] I. De Graeve, H. Terryn, G.E. Thompson, Influence of heat transfer on anodic oxidation of aluminium, J. Appl. Electrochem. 32 (2002) 73–83. doi:10.1023/A:1014229828442.

[68] J.A. González, V. López, A. Bautista, E. Otero, X.R. Nóvoa, Characterization of porous aluminium oxide films from a.c. impedance measurements, J. Appl. Electrochem. 29 (1999)

229–238. doi:10.1023/A:1003481418291.

[69] V. Raj, M.R. Rajaram, G. Balasubramanian, S. Vincent, D. Kanagaraj, Pulse Anodizing - An Overview, Trans. Inst. Met. Finish. 81 (2003) 114–121.

[70] D. Kanagaraj, V. Raj, S. Vincent, B.P. Kumar, A.S. Kumar, S. V Iyer, Pulse anodizing of AA1100 aluminium alloy in oxalic acid electrolyte, Bull. Electrochem. 17 (2001) 285–288. http://cecri.csircentral.net/1232/ (accessed May 22, 2014).

[71] W.E. Cooke, Factors Affecting Loss of Brightness and Image Clarity During Anodizing of Bright Trim Aluminium Alloys in Sulfuric Acid Electrolyte, Plating. (1962) 1157–1164.

[72] H. Takahashi, M. Nagayama, H. Akahori, A. Kitahara, Electron-microscopy of Porous Anodic Oxide Films on Aluminium by Ultra-thin Sectioning Technique: Part 1. The Structrual Change of the Film during the Current Recovery Period, J. Electron Microsc. (Tokyo). 22 (1973) 149–157. http://jmicro.oxfordjournals.org/content/22/2/149.abstract.

[73] M. Nagayama, K. Tamura, Dissolution of the anodic oxide film on aluminium in a sulphuric acid solution, Electrochim. Acta. 12 (1967) 1097–1107. doi:http://dx.doi.org/10.1016/0013-4686(67)80105-1.

[74] M. Nagayama, K. Tamura, H. Takahashi, Dissolution of porous anodic oxide films on Al in (COOH)2 solutions, Corros. Sci. 10 (1970) 617–627. doi:http://dx.doi.org/10.1016/S0010-938X(70)80055-5.

[75] M. Nagayama, K. Tamura, H. Takahashi, Mechanism of open-circuit dissolution of porous oxide films on aluminium in acid solutions, Corros. Sci. 12 (1972) 133–136. doi:http://dx.doi.org/10.1016/S0010-938X(72)90850-5.

[76] Y.S. Kim, S.I. Pyun, S.M. Moon, J.D. Kim, The effects of applied potential and pH on the electrochemical dissolution of barrier layer in porous anodic oxide film on pure aluminium, Corros. Sci. 38 (1996) 329–336. doi:10.1016/0010-938X(96)00131-X.

[77] W. Lin, Anodized aluminum oxide and its application for organic transistors and sensors, 2012.

[78] Z.-P. Tian, K. Lu, B. Chen, Unique nanopore pattern formation by focused ion beam guided anodization., Nanotechnology. 21 (2010) 405301. doi:10.1088/0957-4484/21/40/405301.

[79] V.K. Kommineni, S.P. Harimkar, Pulse electrodeposition of Co-W amorphous coatings, Association for Iron & Steel Technology, 2010.

[80] H.S. Maharana, S. Lakra, S. Pal, A. Basu, Electrophoretic Deposition of Cu-SiO2 Coatings by DC and Pulsed DC for Enhanced Surface-Mechanical Properties, J. Mater. Eng. Perform.

25 (2016) 327–337. doi:10.1007/s11665-015-1834-1.

[81] A. Inesi, Instrumental Methods in Electrochemistry., E. Horwood, 1986. doi:10.1016/0302-4598(86)85047-4.

[82] G. Patermarakis, The origin of nucleation and development of porous nanostructure of anodic alumina films, J. Electroanal. Chem. 635 (2009) 39–50. doi:10.1016/j.jelechem.2009.07.024.

[83] N.Q. Zhao, X.X. Jiang, C.S. Shi, J.J. Li, Z.G. Zhao, X.W. Du, Effects of anodizing conditions on anodic alumina structure, J. Mater. Sci. 42 (2007) 3878–3882. doi:10.1007/s10853-006-0410-3.

[84] S. Ono, M. Saito, M. Ishiguro, H. Asoh, Controlling Factor of Self-Ordering of Anodic Porous Alumina, J. Electrochem. Soc. 151 (2004) B473. doi:10.1149/1.1767838.

[85] A.L. Friedman, D. Brittain, L. Menon, Roles of pH and acid type in the anodic growth of porous alumina, J. Chem. Phys. 127 (2007) 154717. doi:10.1063/1.2790429.

[86] D. Losic, A. Santos, Nanoporous Alumina : Fabrication, Structure, Properties and Applications, Springer International Publishing, 2015. doi:10.1007/978-3-319-20334-8.